RSC Advances

PAPER

View Article Online
View Journal | View Issue

Cite this: *RSC Adv.*, 2024, **14**, 5222

Crystal structure, quantum chemical insights, and molecular docking studies of *N*aryl-2-(*N*-disubstituted) acetamide compounds: potential inhibitors for neurodegenerative enzymes†

Lorena Camargo-Ayala,*[a] Mauricio Bedoya,[bc] Luis Prent-Peñaloza,[d] Efraín Polo-Cuadrado,[a] Edison Osorio,[e] Iván Brito,[f] Gerzon E. Delgado,[fg] Wendy González[hi] and Margarita Gutierrez *[a]

Received 18th December 2023
Accepted 23rd January 2024

DOI: 10.1039/d3ra08649f

rsc.li/rsc-advances

The increase in and concern about neurodegenerative diseases continue to grow in an increasingly long-lived world population. Therefore, the search for new drugs continues to be a priority for medicinal chemistry. We present here the synthesis of a series of compounds with acetamide nuclei. Their structures were established using UV-Visible, NMR, HRMS and IR techniques. Furthermore, we report the crystal structures that were obtained from compounds **5a–5d** by X-ray diffraction. The compounds were evaluated as potential inhibitors of the monoxidase enzymes; A (MAO-A) and B (MAO-B), and cholinesterases; acetylcholinesterase (AChE) and butyrylcholinesterase (BChE) through *in silico* studies using the induced fit docking (IFD) method and binding free energy (ΔG_{bind}) calculations by the MMGBSA method. Interestingly, compounds **5b**, **5c** and **5d** showed much better ΔG_{bind} than the reference drug Zonisamide. Compound **5c** is the best in the series, which indicates a potential selective affinity of our compounds against MAO-B, which could be a promising finding in the search for new drugs for Parkinson's disease treatment. The acetamide crystal exhibits moderate NLO properties suggesting that it could be considered a potential candidate for application in nonlinear optical devices.

1 Introduction

Bioinformatics tools have enabled the description of biological processes through simulations that offer a molecular view of ligand–receptor interactions, providing helpful information for the design and synthesis of new compounds. In addition, with an increasingly aging world population, different types of diseases, including some neurodegenerative disorders, have become significant challenges for medical science that require the use of novel strategies for drug design. Neurodegenerative diseases such as Parkinson's disease (PD) and Alzheimer's disease (AD) still lack safe and efficient treatments.[1,2] Some pharmacological targets such as; monoamine oxidase (A:MAO-A and B:MAO-B), whose inhibitors have been used for the treatment of psychiatric and neurological disorders, respectively,[3] and cholinesterases; butyrylcholinesterase (BChE) and acetylcholinesterase (AChE) associated with AD[4] have been identified. MAO-B is involved with the breakdown of dopamine, a neurotransmitter related to PD.[5] The molecular elucidation and the identification of the active sites of these enzymes have allowed us to determine how some ligands can modulate them successfully, which allows us, through a well-founded analysis, to establish the necessary characteristics for the synthesis of new compounds

[a]*Laboratorio Síntesis Orgánica y Actividad Biológica (LSO-Act-Bio), Instituto de Química de Recursos Naturales, Universidad de Talca, Casilla 747, Talca 3460000, Chile. E-mail: loreca17@gmail.com*

[b]*Centro de Investigación de Estudios Avanzados del Maule (CIEAM), Vicerrectoría de Investigación y Postgrado, Universidad Católica del Maule, Talca 3466706, Chile. E-mail: mgutierrez@utalca.cl*

[c]*Laboratorio de Bioinformática y Química Computacional (LBQC), Departamento de Medicina Traslacional, Facultad de Medicina, Universidad Católica del Maule, Talca 3466706, Chile*

[d]*Departamento de Ciencias Químicas, Facultad de Ciencias Exactas, Universidad Andrés Bello, Quillota 980, Viña del Mar, Chile*

[e]*Facultad de Ciencias Naturales y Matemáticas, Universidad de Ibagué, Carrera 22 Calle 67, Ibagué 730001, Colombia*

[f]*Departamento de Química, Facultad de Ciencias B, á, sicas, Universidad de Antofagasta, Campus Coloso, Antofagasta 02800, Chile*

[g]*Departamento de Química, Facultad de Ciencias, Universidad de Los Andes, Mérida 5101, Venezuela*

[h]*Centro de Bioinformática y Simulaciones Moleculares (CBSM), Universidad de Talca, Casilla 747, Talca 3460000, Chile*

[i]*Facultad de Ingeniería and Millennium Nucleus of Ion Channels-Associated Diseases (MiNICAD), Universidad de Talca, 3460000 Talca, Chile*

† Electronic supplementary information (ESI) available. CCDC 2211917, 2211918, 2238258 and 2238259. For ESI and crystallographic data in CIF or other electronic format see DOI: **https://doi.org/10.1039/d3ra08649f**

that can interact with these specific targets due to their structural features.

Acetamide-type compounds have been shown to be potent modulators of MAO-A, MAO-B, AChE, and BChE. Recently, a potent and selective MAO-A inhibitor (50 times more selective over MAO-A) was reported, *N*-[5-(acetyloxy)-2-(4-chlorophenyl)-4-oxo-4,5-dihydropyrazolo[1,5-*a*]quinoxalin-7-yl]acetamide, the compound showed an IC_{50} value of 0.028 μM.[6] On the other hand, milacemide and its structural modifications; alpha-milacemide or safinamide (Fig. 1), are inhibitors of the enzyme MAO-B, which plays an important role in the exacerbation of PD.[7,8] In addition, triazole derivative compounds linked to benzothiazole through an acetamide linker,[9] naphthoquinone conjugated to aryltriazole acetamide derivatives[10] and the compound *N*-(naphthalen-1-yl)-2-(piperidin-1)-acetamide,[11] recently reported by our group, have shown inhibitory activity against AChE and/or BChE. Furthermore, in recent studies, it has been reported that a series of compounds (*R*)-*N*-(benzo[*d*]thiazol-2-yl)-2-(1-phenyl-3,4-dihydroisoquinolin-2(1*H*)-yl)acetamide showed potent specific inhibitory polypharmacological activity against MAO-B and BChE.[12]

Different synthesis strategies have been proposed to obtain amides. The classic strategies, such as; the reaction between the carboxylic acid and the amine,[13] or seeking to avoid the acid-base balance, the formation of salts and improve yields, the synthesis from the acyl chloride, which requires a previous synthetic step for the formation of the halide and strong conditions due to its reactivity.[14] Other synthetic strategies involve the activation of the acid for the coupling with the amine using a coupling reagent. These reagents, such as carbodiimides, have proven efficient for forming amides,[15] resulting in amidations with high yield and selectivity.[16] The most widely used carbodiimides industrially are DCC (*N*,*N*′-dicyclohexylcarbodiimide, DIC (*N*,*N*′-diisopropylcarbodiimide), and EDC (1-ethyl-3-(3′-dimethylaminopropyl)carbodiimide hydrochloride).[16]

However, the choice of the coupling reagent must consider some limitations; for example, the use of DCC generates as a by-product *N*,*N*′-dicyclohexylurea, which is insoluble in water, and although it can be removed by filtration, it has been shown to be challenging to remove from reactions in solution because small traces remain, even after purification by column chromatography.[17] These last typical drawbacks of DCC are mostly overcome when DIC is used as a coupling reagent.[18] Another alternative is the use of EDC, which generates water-soluble urea as a by-product that is easy to eliminate. However, it has a high cost, which makes it challenging to access.[16] DIC is more accessible and has shown better yields in some reactions compared to EDC.[19] In this context, a series of acetamide compounds, their synthesis, crystal structure and computational studies are presented here to describe their possible activity against MAO-A, MAO-B, AChE and BChE enzymes.

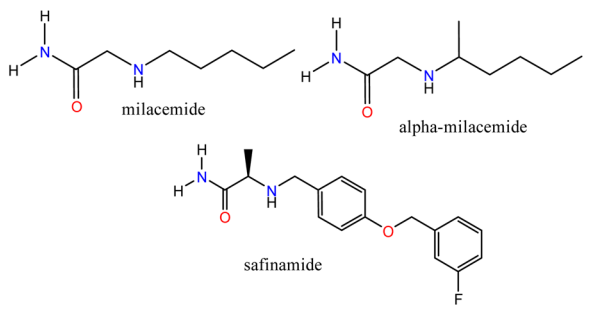

Fig. 1 Acetamide-type compound modulators of MAO-B.

2 Results and discussion

2.1 Chemistry

Initially, compounds **5a–5d** were synthesized in two reaction steps. Thus, reagents 1 (carboxylic acid) and 2 (aromatic amine) were combined to generate compound 3, for which DIC was used as the coupling reagent. Product 3 was purified and dried. The next stage consisted of the reaction between the product obtained in the first phase and 4 (aliphatic amine) to obtain compounds **5a–5d**. Finally, the compounds were purified by column chromatography using ethyl acetate:petroleum ether mixtures as eluant and left in solution to evaporate to crystals. The compounds were obtained with moderate to good yields (Table 1).

2.2 X-ray diffraction measurements

The title compounds crystallized with orthorhombic (**5a**) and monoclinic symmetry (**5b–5d**), respectively, with one or two (**5c**) independent molecules in the asymmetric unit. Fig. 2 shows the molecular conformation and atom labeling of the asymmetric unit in the title compounds. In the structures, all bond distances and angles are normal[20] and agree with the average values in similar entries found in the Cambridge Structural Database CSD, version 5.43, November 2022.[21] As expected, the amide bond in the molecules is nearly planar and *trans*-configurated.

The molecular structure and crystal packing of all molecules are stabilized by intermolecular N–H···O hydrogen bonds (Table 2). For **5a**, **5b**, infinite one-dimensional chains are formed along [010] direction, and for **5d** the chains run along [001] direction. These chains are parallel to each other (Fig. 3), which can be described in graph-set notation as C(4).[22] For **5c**, each independent molecule form intramolecular bonds with graph-set notation *S*(5). All crystal structures remain united due to van der Waals forces.

Table 3 summarizes both compounds' crystal data, intensity data collection, and refinement details. X-ray crystal structure determinations, CIF files containing tables of crystallographic parameters, bond lengths, and bond angles, as well as a list of structure factors have been deposited in the Cambridge Crystallographic Data center (CCDC no. 2211917, 2211918, 2238258, and 2238259). They are freely available upon request from the following website: **www.ccdc.cam.ac.uk/data_request/cif**.

2.3 Computational analyses

2.3.1 Comparison of geometry data. The root mean squared (RMS) values predicted by Chemcraft software, which accounts for the difference between the monomer from X-ray

Table 1 Crystal structure of compounds **5a–5d**

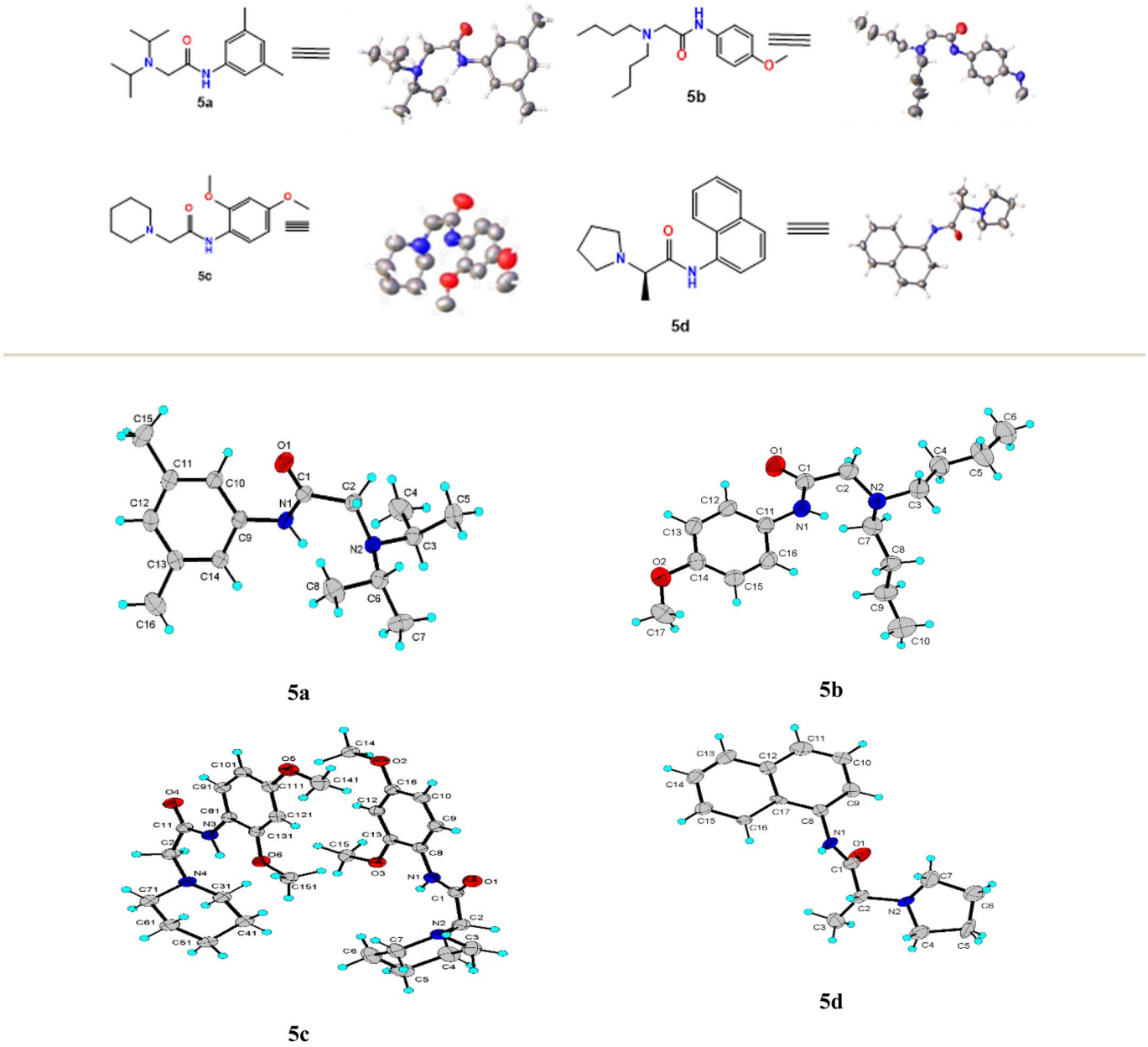

Fig. 2 Asymmetric unit for each compound with anisotropic ellipsoid representation, together with atom labeling scheme. The ellipsoids are drawn at 30% probability level, hydrogen atoms are depicted as spheres with arbitrary radii.

Table 2 Parameters (distance: Å, angle: °) for short intermolecular and intramolecular contacts. (D-donor; A-acceptor; H-hydrogen)

Compound	D–H···A	D–H	H···A	D···A	D–H···A	Symmetry
5a	N1–H1···O1	0.860	2.400	3.179(2)	152.0	$1/2 - x, -1/2 + y, z$
5b	N1–H1···O1	0.860	2.450	3.211(2)	148.0	$x, -1 + y, z$
5c	N3–H3···O6	0.830	2.110	2.576(2)	107.0	x, y, z
5d	N1–H1···O1	0.860	2.030	2.88(2)	167.0	$-1 + x, y, z$

diffraction experiment and the theoretically optimized geometry were relatively low: 0.455 Å for **5a**, 0.3730 Å for **5b**, 0.587 Å for **5c** and 0.797 Å for **5d**. Then, a good agreement was found between the optimized molecular geometrical parameters and experimental ones. The coordinates and chemical bonding distances can be download from ESI.†

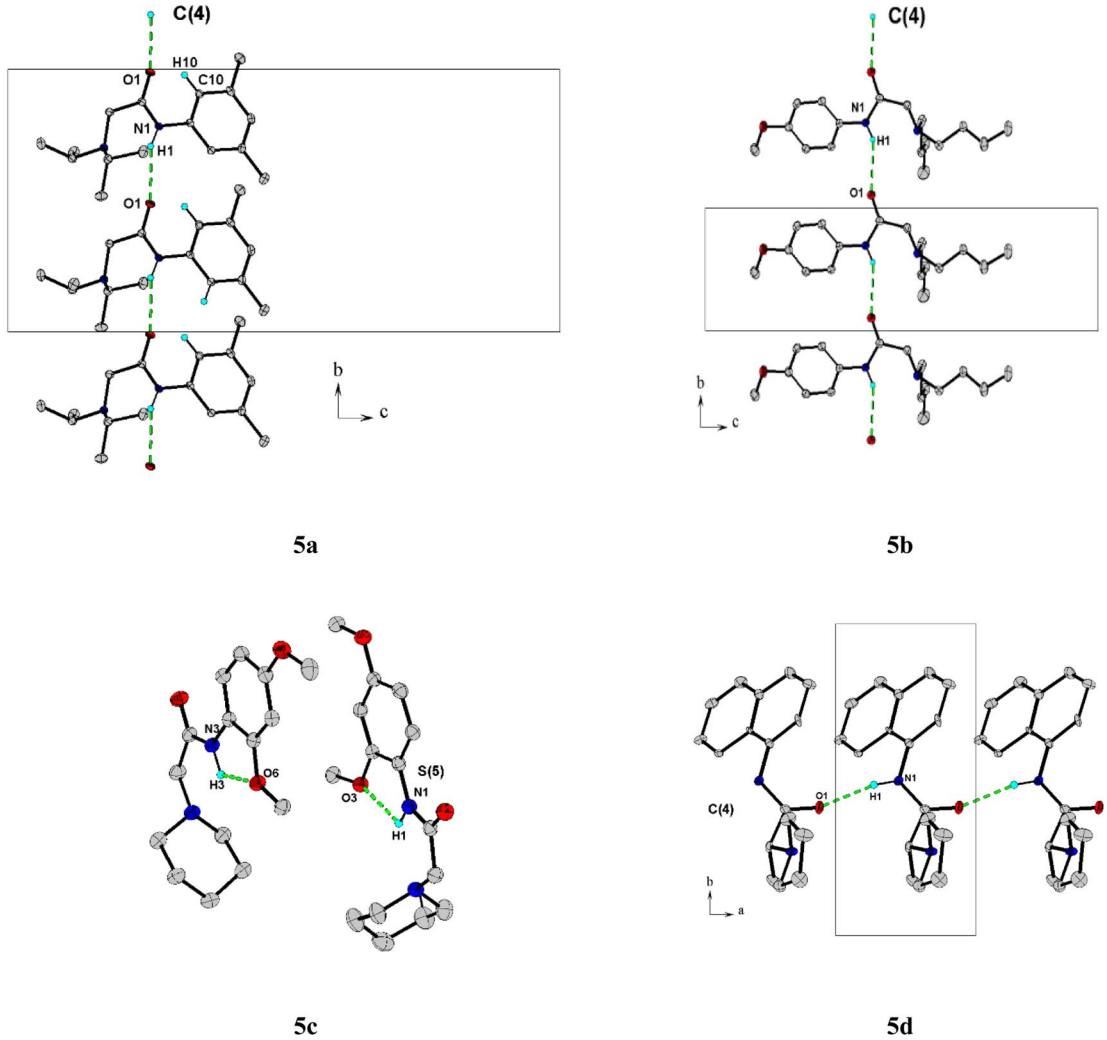

Fig. 3 A partial view of the crystal packing of **5a**, **5b**, **5c**, and **5d**. Intermolecular hydrogen bonds, N–H···O, are indicated by dashed lines. H atoms not involved in hydrogen bonding have been omitted for clarity.

2.3.2 UV-vis studies and electronic properties. The experimental and theoretical absorption spectra are presented in Fig. 4. All experimental absorption spectra are located between 260 and 330 nm, with absorption maxima of 272 nm for **5a**, 282 nm for **5b**, 288 nm for **5c** and 290 nm for **5d**. Regarding the absorption spectra obtained theoretically, the first electronic transition signals are close to the maximum absorption values obtained experimentally: 268 nm for **5a**, 272 nm for **5b**, 274 for **5c** and 313 for **5d**. As a general comment, the calculated absorbance value does not match exactly the experimental values because these measurements are directly proportional to the sample concentration, which cannot be calculated in our Gaussian experiment. To obtain absorbance values close to the experimental ones is necessary to model different geometrical conformations using explicit solution methods involving a long computational process, which is an unintended goal of this work.

2.3.3 Frontier molecular orbitals (FMOs) analysis and molecular reactivity. The HOMO and LUMO energies, frontier orbital energy gap, chemical hardness, chemical potential, electrophilicity index, and chemical softness parameters for **5a**–**5d** compounds are presented in Table 4 and Fig. 5. The Homo–Lumo Gap and chemical hardness are measurements of stability for a chemical system: high values mean resistance to changes in electron density, which gives insight into the reactivity of the molecules. The highest stabilities are presented for **5a**, **5b** and **5c** molecules. On the other hand, the chemical potential (μ) and electrophilicity (ω) measures the stabilization in energy when the system acquires an additional electronic charge ΔN from the environment. The highest values are reported for **5d**, which means this compound is stabilized after a chemical reaction. Finally, compounds with high chemical reactivity and low stability are considered soft, thus **5d** can be considered the softest molecule among them.

2.3.4 Nonlinear optical (NLO) properties. The dipole moment, polarizability and hyperpolarizability results obtained at CAM-B3LYP/def2tzvp level of theory is presented in Table 5. Urea as well as three published compounds with NLO properties have been used as prototype molecules for a comparative approach to NLO properties. The relevance of polarizability and

Table 3 X-ray crystallographic data and structural refinement for compounds **5a–5d**

Compound	**5a**	**5b**	**5c**	**5d**
CCDC number	2 211 918	2 211 917	2 238 259	2 238 258
Empirical formula	$C_{16}H_{26}N_2O$	$C_{17}H_{28}N_2O_2$	$C_{30}H_{44}N_4O_6$	$C_{17}H_{17}N_2O$
Formula weight	262.39	292.41	556.69	265.32
Temperature/K	298	298	298	298
Crystal system	Orthorhombic	Monoclinic	Monoclinic	Monoclinic
Space group	*Pbca*	$P2_1/n$	$P2_1/c$	*P*21
a/Å	14.1335(11)	15.9867(9)	7.1033(4)	4.763(7)
b/Å	10.5456(7)	5.3642(3)	23.7608(14)	10.544(16)
c/Å	22.1248(17)	21.1924(11)	18.3655(11)	15.14(2)
β/°	—	103.788(2)	93.527(4)	96.49(4)
Volume/Å^3	3297.6(4)	1765.00(17)	3093.9(3)	756(2)
Z	8	4	4	2
*ρ*calcg/cm^3	1.057	1.100	1.195	4.763(7)
μ/mm 1	0.066	0.072	0.678	0.074
F(000)	1152	640	1200.0	288
Crystal size/mm^3	0.14 × 0.22 × 0.32	0.16 × 0.24 × 0.40	0.14 × 0.18 × 0.35	0.15 × 0.20 × 0.30
Radiation	MoK*α* ($\lambda = 0.71073$)	MoK*α* ($\lambda = 0.71073$)	CuK*α* ($\lambda = 1.54178$)	MoK*α* ($\lambda = 0.71073$)
Flack	—	—	—	−0.6(1)
2*Θ* range for data collection/°	5.16 to 61.072	5.248 to 58.302	8.87 to 150.136	2.7 to 26.5
Index ranges	$-20 \le h \le 20$, $-15 \le k \le 14$, $-31 \le l \le 31$	$-21 \le h \le 21$, $-7 \le k \le 7$, $-29 \le l \le 28$	$-8 \le h \le 8$, $-29 \le k \le 29$, $-22 \le l \le 22$	$-5 \le h \le 5$, $-12 \le k \le 13$, $-18 \le l \le 18$
Reflections collected	74 427	53 960	55 156	5760
Independent reflections	5034 [$R_{int} = 0.3243$]	4749 [$R_{int} = 0.0839$]	6289 [$R_{int} = 0.102$]	2031 [$R_{int} = 0.410$]
Data/restraints/parameters	5034/0/183	4749/0/212	6289/0/376	2031/0/182
Goodness-of-fit on F2	0.860.16	1.094	1.029	0.87
Final *R* indexes [$I \ge 2\sigma(I)$]	$R_1 = 0.0670$, w$R_2 = 0.1273$	$R_1 = 0.0796$, w$R_2 = 0.1952$	$R_1 = 0.0643$, w$R_2 = 0.2058$	$R_1 = 0.0847$, w$R_2 = 0.1474$
Largest diff. peak/hole/eÅ^{-3}	0.18/−0.18	0.58/−0.75	0.23/−0.17	0.16/−0.16

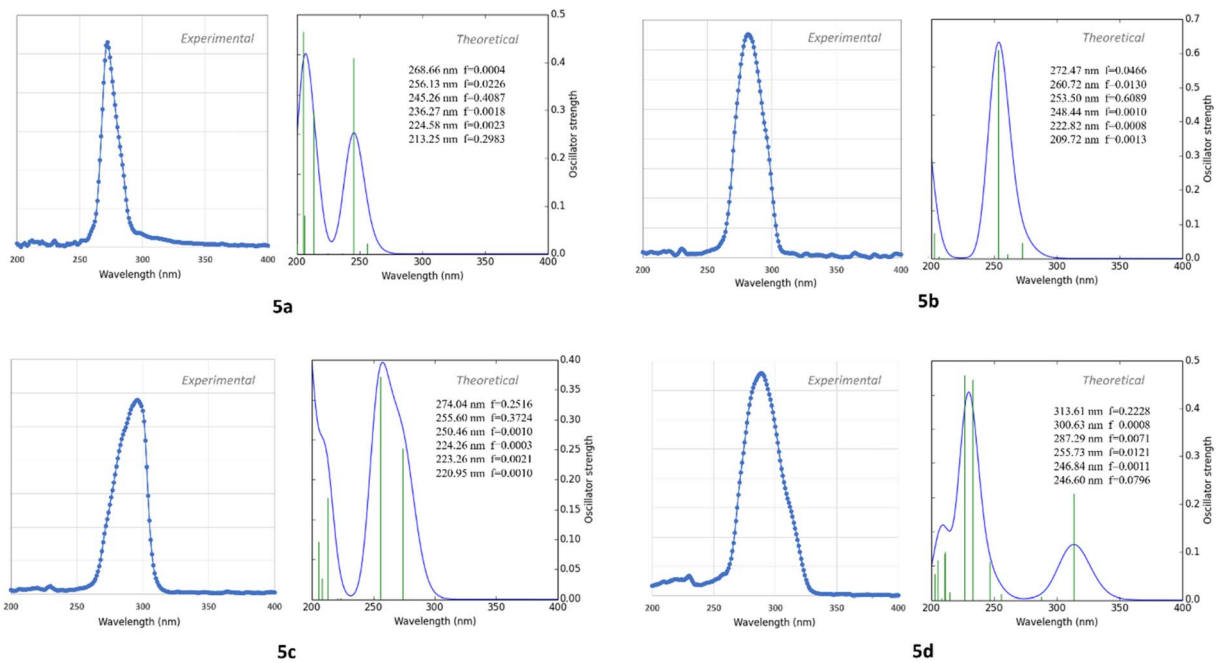

Fig. 4 Experimental and calculated electronic absorption spectra for compounds, from **5a** to **5d**.

Table 4 Chemical reactivity descriptors from density functional theory[a]

Compound	HOMO	LUMO	HOMO–LUMO gap	Chemical hardness (η)	Chemical potential (μ)	Electrophilicity index (ω)	Chemical softness (s)
5a	−7.2309	0.5254	7.76	3.88	3.35	1.45	0.13
5b	−6.8886	0.5703	7.46	3.73	3.16	1.34	0.13
5c	−6.6692	0.7923	7.46	3.73	2.94	1.16	0.13
5d	−7.1087	−0.5929	6.52	3.26	3.85	2.28	0.15

[a] All values are in eV.

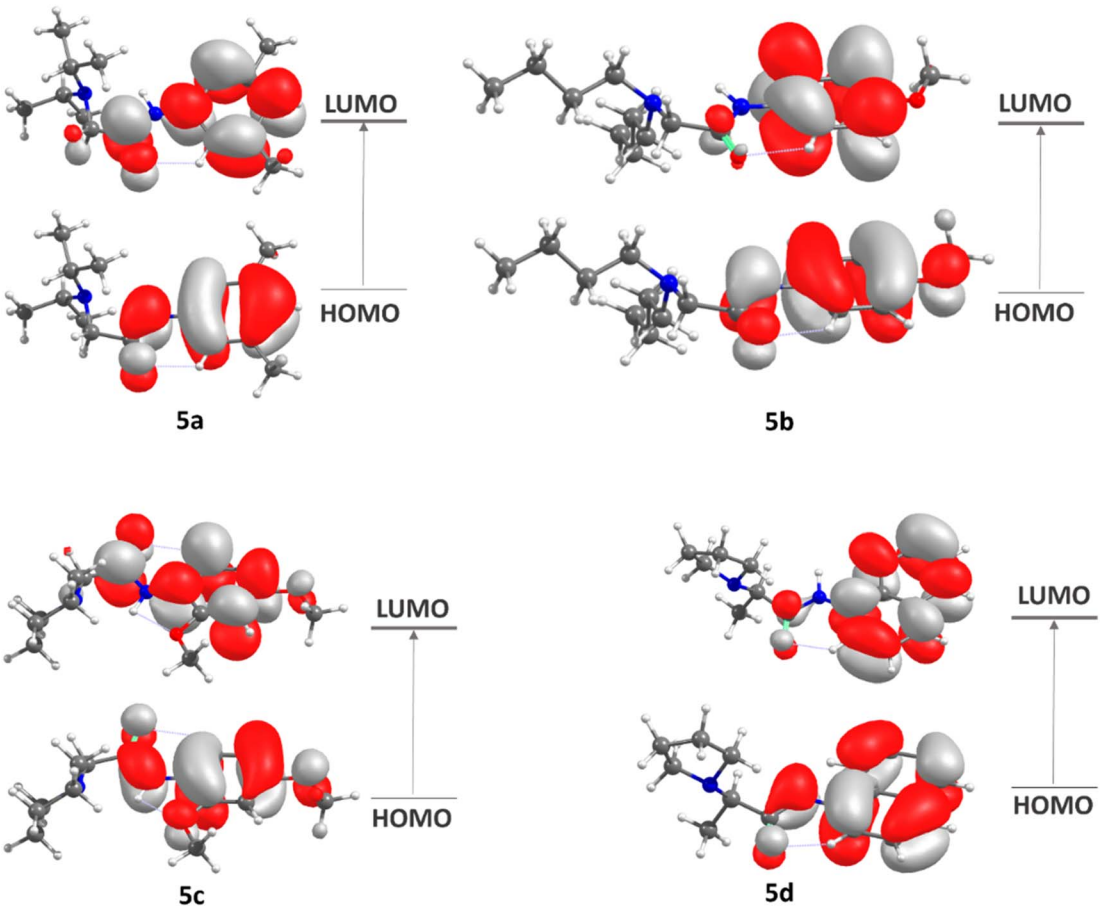

Fig. 5 HOMO–LUMO diagrams for **5a** to **5d**.

hyperpolarizability of a molecular system depends on electronic communication between two distinct parts of a molecule. The results showed non-zero μ values for all compounds, which should cause microscopic quadratic and cubic hyperpolarizabilities, with resulting non-zero values derived by the second numerical derivatives of electric dipole moments to the field implemented (see Table 5). The high second hyperpolarizability (γ) values presented by all compounds, compared with urea, are an indicative that all systems shows a strong nonlinear optical effects, crucial for advanced nonlinear optical applications, particularly in all-optical signal processing, optical switching, and the development of highly efficient nonlinear optical devices. Our crystalized molecules were compared again 2-(4-chlorophenyl)-*N*-(pyrazin-2-yl) acetamide (CNPA), whose molecular structure and the supramolecular assembly were determined by Narayana *et al.*[23] In all cases, from **5a** to **5d** molecules, the dipole moment, polarizability and hyperpolarizability values are higher than CNAP acetamide.

2.3.5 Theoretical inhibition. To validate the molecular docking protocol with IFD and re-scoring of the molecular docking poses by MMGBSA calculations, the crystallized reference ligands were re-docked into their original structure. Table 6 shows the RMSD value of the reference ligand with respect to the pose with the most favorable binding free energy (ΔG_{bind}). The RMSD values are below 2 Å which is a criterion of the protocol's predictive power.

Table 5 Dipole moment, polarizability and hyperpolarizability values obtained at CAM-B3LYP/6-311++g(d,p) level of theory

Compounds	μ (D)	α ($\times 10^{-24}$ esu)	β ($\times 10^{-30}$ esu)	γ ($\times 10^{-36}$ esu)
5a	4.202	31.046	1.891	27.477
5b	6.330	30.229	4.920	28.676
5c	5.332	33.760	4.737	30.277
5d	3.687	32.329	3.444	31.798
Urea	3.875	4.823	0.414	2.941
CNPA acetamide as reference[23]	2.490	24.081	1.721	16.179

Table 6 Crystallographic structures used, reported inhibitory activity, and RMSD values from IFD redocking and MMGBSA validation

PDB ID	Protein	Ligand	RMSD (Å)	Affinity
2Z5X (ref. 24)	MAO-A	Harmine	0.66	ki = 0.005 ± 0.0002 μM (ref. 25)
3PO7 (ref. 26)	MAO-B	Zonisamide	0.45	ki = 3.1 ± 0.3 μM (ref. 26)
4BDT (ref. 27)	AChE	Huprine W	1.32	IC_{50} = 1.1 ± 0.1 nM (ref. 28)
4BDS (ref. 27)	BChE	Tacrine	0.74	Ki = 12 nM (ref. 29)

The ΔG_{bind} obtained by MMGBSA method is shown in Table 7with the reference ligands in each system. The ΔG_{bind} values for the compounds studied in MAO-A are less negative than the reference ligand (harmine), indicating that they are potentially less active than the harmine compound.

For MAO-B, on the other hand, the ligands studied present a range of ΔG_{bind} values (−54.81; −74.53 kcal mol^{-1}) more negative than the reference ligand zonisamide (−34.73 kcal mol^{-1}), which makes them potentially more affine than zonisamide, with **5c** being the ligand with the highest probability of having an action on MAO-B. The compounds studied presented less negative ΔG_{bind} values in AChE with respect to the huprine-W compound, however, compound **5d** presented a ΔG_{bind} value of −68.75 in BChE, quite close to the energetic value of the tacrine compound. As reported for the MAO-B – zonisamide complex, compound **5c** also has no direct interaction with the FAD cofactor and furthermore maintains two important hydrophobic interactions with residues TYR326 and LEU171.[26] Zonisamide interacts with its benzyl group while **5c** interacts with the aromatic ring that is oriented in the same plane as the benzyl moiety of zonisamide, retaining the same hydrophobic interactions (Fig. 6).

Table 7 Binding free energy calculated with the MMGBSA method

	ΔG_{bind} (kcal mol^{-1})			
Compound	MAO-A	MAO-B	AChE	BChE
5a	−67.43	−54.81	−71.24	−58.30
5b	−73.25	−72.50	−68.49	−42.94
5c	−61.89	−74.53	−65.35	−55.48
5d	−64.83	−72.72	−78.38	−68.75
Harmine	**−80.49**	—	—	—
Zonisamide	—	**−34.73**	—	—
Huprine W	—	—	**−114.13**	
Tacrine	—	—	—	**−69.82**

Among the key interactions between tacrine and BChE are a π–π stacking interaction between the aromatic ring of tacrine and residue TRP82, a hydrogen bond between the NH group of

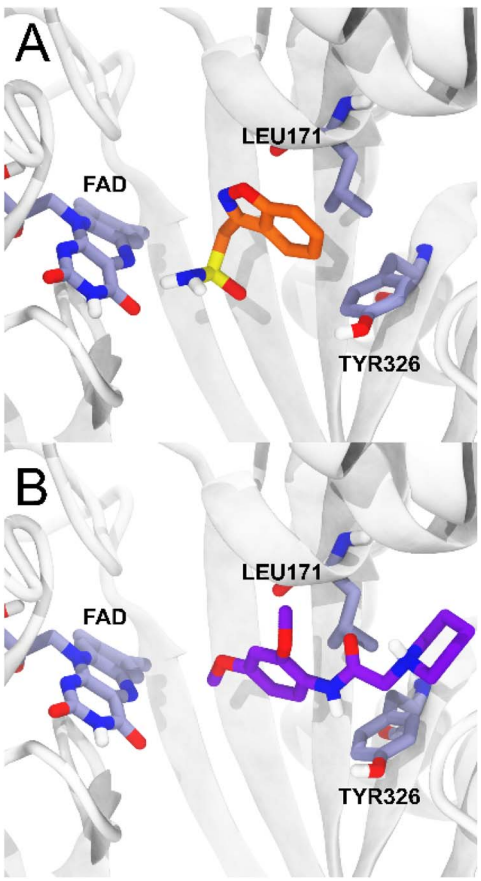

Fig. 6 MAO-B complexes. (A) The crystallographic structure of zonisamide is shown in orange and the binding site residues in light purple. (B) Binding mode of compound **5c** obtained by IFD and MMGBSA calculations. Compound **5c** is shown in purple.

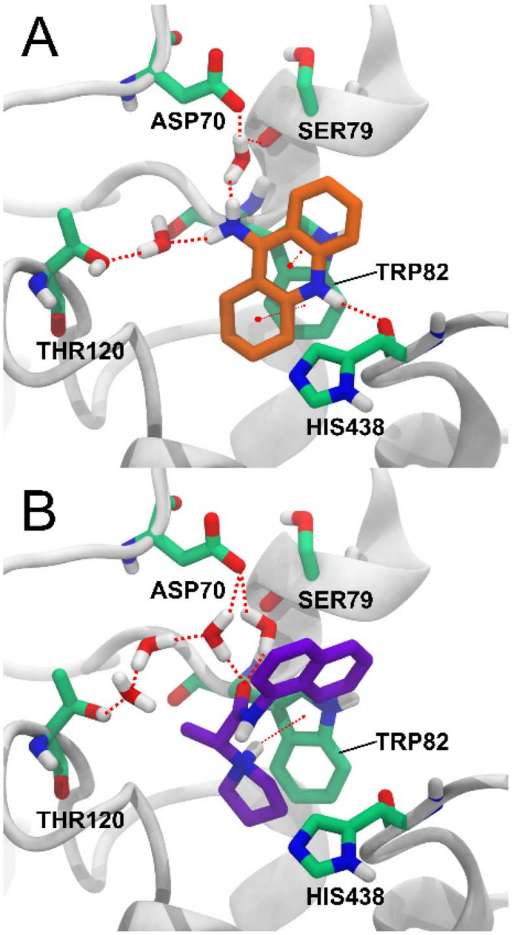

Fig. 7 BChE complexes. (A) The crystallographic structure of tacrine is shown in orange and the binding site residues in green. (B) Binding mode of compound **5d** obtained by IFD and MMGBSA calculations. Compound **5d** is shown in purple.

tacrine and the carbonyl of residue HIS438, and a hydrogen bond between the amino group of tacrine and two water molecules that simultaneously form hydrogen bonds with ASP70, SER79 and THR120.[27] Of these interactions, compound **5d** also forms a π – cation interaction with residue TRP82 with the charged amino group of **5d** and forms a water bridge network between the carbonyl group and the residues ASP70 and THR120. The interaction with residue THR120 is not *via* a single water molecule as in tacrine but *via* three water molecules (Fig. 7). Water-mediated hydrogen bonding networks have been shown to be crucial in ligand–protein interactions, but their stability and the effect of their displacement are difficult to determine.[30] Therefore, the interaction between compound **5d** and THR120 mediated by 3 water molecules may not be stable or strong enough.

3 Conclusions

In summary, we synthesized compounds with acetamide nuclei through coupling reagents. The products were obtained with moderate to good yields with high purity. The compounds were elucidated by NMR (^{1}H and ^{13}C), IR, HRMS and X-ray crystallography. The crystals of compounds **5a**, **5b**, **5c** and **5d** showed a monoclinic and orthorhombic system in which the amide bond in the molecules is almost flat and *trans*-configured, stabilized by hydrogen bonds. The *in silico* analyses of the compounds as biological inhibitors against MAO-A, MAO-B, AChE and BChE did not show a better affinity for the MAO-A, AChE and BChE enzymes than the drugs used as a reference, except for compound **5d**. which showed interactions and affinity similar to tacrine (reference drug used for BChE); a π – cation interaction with the TRP82 residue and a water bridge network between the carbonyl group and the ASP70 and THR120 residues. All the compounds showed a high affinity for MAO-B as well in the *in silico* studies, and all the compounds of

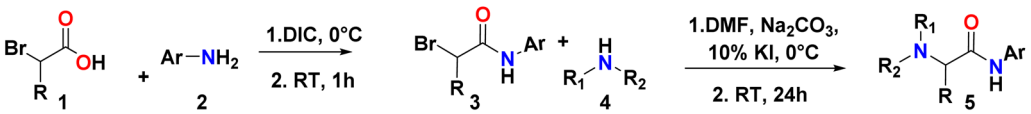

Entry	-Ar	-R	-R$_1$=R$_2$	Yield (%)
5a	- 3,5 -Me-C$_6$H$_3$	-H	Isopropyl	73.65
5b	-4-MeO- C$_6$H$_4$	-H	Butyl	66.88
5c	-2,4-MeO- C$_6$H$_3$	-H	Piperidine	89.48
5d	-naphthyl	-Me	Pyrrolidine	82.00

Scheme 1 Compound synthesis **5a** to **5d**.

the series studied presented a range of ΔG_{bind} values more negative than the reference ligand zonisamide, which makes them potentially more related to MAO-B. Compound **5c** showed the most negative ΔG_{bind} value (−74.53 kcal mol^{-1}) *versus* ΔG_{bind} for zonisamide (−34.73 kcal mol^{-1}), which indicates a greater probability of having an action on MAO-B. Molecular docking analysis showed compound **5c** tends to be the most related to MAO-B, since it presents similar interactions to zonisamide, maintaining two hydrophobic interactions with residues TYR326 and LEU171 and interacting with the aromatic ring instead of a benzyl group. The *in silico* analyses suggest that compounds **5a–5d** could serve as a scaffold for structural diversification seeking to improve the efficacy of MAO-B enzymatic inhibition. Therefore, the synthesis of compounds **5a–5d** becomes an interesting finding in the search for selective drugs for the treatment of the Parkinson's disease.

Moreover, based on the magnitude of the hyperpolarizability measurement, we conclude that **5a**, **5b**, **5c** and **5d** offers potential applications to the development of materials with NLO properties, making them potentially valuable for applications in advanced optics and photonics. The comparison with urea and CNPA acetamide compounds indicates their potential superiority for certain nonlinear optical applications.

4 Materials and methods

For the reactions, the reagents, solvents, and other materials used were provided by Sigma-Aldrich and Merck. To monitor the reactions, thin layer chromatography (TLC) was used using GF254 silica Al TLC plates. The spots were revealed using a SPECTROLINE MODEL CM-10 camera (254 and 366 nm) and/or developing solutions. For the characterization of the compounds, infrared (IR) spectra (KBr pellets, 500–4000 cm^{-1}) were taken on a NEXUS 670 FT-IR spectrophotometer (Thermo Nicolet, Madison, WI, USA). Nuclear magnetic resonance (NMR) spectra were obtained on a Bruker DPX 400 spectrometer (400 MHz for ^{1}H and 100 MHz for ^{13}C). Samples were dissolved in $CDCl_3$ and tetramethylsilane (TMS) was used to calibrate the signals. The displacement (δ) and coupling constant (J) values are expressed in parts per million (ppm) and Hertz (Hz), respectively. The signals were represented as singlet (s), doublet (d), triplet (t) and multiplet (m). HRMS spectra were performed on a Bruker Compact QqTOF spectrometer. The analysis was performed by direct injection. A 500 μL Hamilton syringe was used for injection, with a flow rate of 2 μL min^{-1} using the InfusionONE Syringe Pump NE-300. For ionization, an ESI source was used, with a voltage of 4500 V, a gas temperature of 180 °C, flow at 4 L min^{-1}, and a nebulizer at 0.4 bar. The purity of the compounds was verified using high-performance liquid chromatography (HPLC), for which a C-18 reverse phase column LiChroCart 125-4 LiChrospher 100 RP-18 (5 μM) was used. For the mobile phase, two solutions were used; the first (solution A) was a 0.1% solution of trifluoroacetic acid (TFA) in acetonitrile (CH_3CN), and the second (solution B) was a 0.1% aqueous TFA mixture. The flow rate was 1 mL min^{-1}, and the chromatograms were acquired at a wavelength of 254 nm. For this, the YL9100 instrument was used with a YL9110 quaternary pump, a YL9150 autosampler, a YL9101 degassing pump, and a photodiode array (PDA) detector. YL9160 (190–400 nm), manufactured by YL INSTRUMENT CO, LTD. The analyzes were performed with the Clarity software version 6.0 of 2012. Melting points (m.p.), uncorrected, were measured on an IA9100 electrothermal apparatus (Stone, Staffs, UK) in triplicate.

4.1 Synthesis of compounds 5

The synthesis was carried out in two steps (Scheme 1); in the first step, the amidation was carried out by mixing carboxylic acid (**1**) (1 mmol, 1 equiv.) in dichloromethane (DCM) at 0 °C with the aromatic amine (**2**), previously DIC (170.33 μL, 1.1 equiv.) was added to the acid, and it was stirred for 2 minutes. The reaction was followed by TLC and the reaction crude was purified using column chromatography. In the second step, potassium iodide (KI) and sodium car-bonate (Na_2CO_3) (10 mol% and 1 mmol, 1 equiv.) were add-ed to the amide product (**3**) and dissolved in DMF at 0 °C. Then, the aliphatic amine (**4**) (1.3 mmol, 1.3 equiv.) was added in DCM. After 24 h at room temperature, extraction with ethyl acetate (50 mL) was carried out, followed by washings with water, a saturated sodium bicarbonate solution and a saturated sodium chloride solution (20 mL in each case) and subsequently dried with anhydrous Na_2SO_4. The final prod-ucts (**5a–5d**) were isolated by column chromatography. For crystallization, the compounds were redissolved in DCM and left to stand in a mixture of DCM : petroleum ether (1 : 1) for **5a**, **5c** and **5d**, and petroleum ether : ethyl acetate (7 : 3) for **5b**, until the formation of the crystal.

4.1.1 2-(diisopropylamino)-*N*-(3,5-dimetylphenyl)acetamide (5a). ^{1}H- NMR (400 MHz, $CDCl_3$) δ 9.43 (s, 1*H*), 7.23 (s, 2*H*), 6.78 (s, 1*H*), 3.18 (s, 2*H*), 3.13–3.17 (m, 2*H*), 2.34 (s, 6*H*), 1.11 (d, J = 6.5 Hz, 12*H*); ^{13}C-NMR (100 MHz, $CDCl_3$) δ: 171.4 (C), 138.7 (C), 137.5 (C), 125.7 (CH), 116.8 (CH), 50.3 (CH_2, CH), 21.3 (CH_3), 20.6 (CH_3); IR (KBr): ν: 3259.70, 2966.52, 2866.22, 2360.87, 1670.35, 1608.63, 1527.62, 775.38 cm^{-1}; HRMS (ESI, m/z): Calcd for $C_{16}H_{26}N_2O$ $[M + H]^+$ 263.2123 found 263.2120; HPLC Purity = 96.6% ((Solution A: (TFA 0.01%/acetonitrile) y (Solution B: TFA 0.01%)), 1 mL min^{-1}, tR = 3.740 min). Yellow solid; Yield: 73.65%; m.p = 58-59 °C.

4.1.2 2-(dibutylamino)-*N*-(4-methoxiphenyl)acetamide (5b). ^{1}H-NMR (400 MHz, $CDCl_3$) 9.27 (s, 1*H*), 7.48 (d, J = 8 Hz, 2*H*), 6.88 (d, J = 12 Hz, 2*H*), 3.79 (s, 3*H*), 3.14 (s, 2*H*), 2.65–2.43 (m, 4*H*), 1.53–1.41 (m, 4*H*), 1.38–1.24 (m, 4*H*), 0.93 (t, J = 7.3 Hz, 6*H*); ^{13}C-NMR (100 MHz, $CDCl_3$) δ: 169.7 (C), 156.1 (C), 131.1 (C), 120.7 (CH), 114.2 (CH), 59.2 (CH_2), 55.5 (CH_3), 55.2 (CH_2), 29.5 (CH_2), 20.6 (CH_2), 14.0 (CH_3); IR (KBr): ν: 3278.99, 2997.38, 2954.95, 2862.36 2831.50, 1666.50, 1593.20, 1527.62, 779.24 cm^{-1}; HRMS (ESI, m/z): Calcd for $C_{17}H_{28}N_2O_2$ $[M + H]^+$ 293.2229 found 293.2225; HPLC Purity = 98.2% ((Solution A: (TFA 0.01%/acetonitrile) y (Solution B: TFA 0.01%)), 1 mL min^{-1}, tR = 3.393 min). White solid; Yield: 66.88%; m.p = 50-51 °C.

4.1.3 *N*-(2,4-dimethoxyphenyl)-2-(piperidin-1-yl)acetamide (5c). ^{1}H-NMR (400 MHz, $CDCl_3$) 9.66 (s, 1*H*), 8.28–8.17 (m, 1*H*), 6.47 (m, 2*H*), 3.86 (s, 3*H*), 3.79 (s, 3*H*), 3.07 (s, 2*H*), 2.53 (bs, 4*H*), 1.64 (m, 4*H*), 1.52–1.40 (m, 2*H*); ^{13}C- NMR (100 MHz, $CDCl_3$)

δ 168.4 (C), 156.3 (C), 149.7 (C), 121.2 (CH), 120.4 (C), 103.7 (CH), 98.7 (CH), 62.8 (CH_2), 55.7 (CH_3), 55.5 (CH_3), 54.8 (CH_2), 26.4 (CH_2), 23.7 (CH_2). IR (KBr): ν: 3275.13, 3248.13, 2924.09, 2850.79, 2758.21, 1681.93, 1600.92, 1567.62, 817.82 cm^{-1}; HRMS (ESI, m/z): Calcd for $C_{15}H_{22}N_2O_3$ $[M + H]^+$ 279.1709 found 279.1714; HPLC Purity = 98.2% ((Solution A: (TFA 0.01%/acetonitrile) y (Solution B: TFA 0.01%)), 1 mL min^{-1}, tR = 3.400 min). Yellow solid; Yield: 89, 48%; m.p= 70-71 °C.

4.1.4 (*R*)-*N*-(naphthalen-1-yl)-2-(pyrrolidin-1-yl) propanamide (5d). ^{1}H-NMR (400 MHz, $CDCl_3$) δ 9.74 (s, 1*H*), 8.18 (d, J = 7.4 Hz, 1*H*), 7.86–7.81 (m, 1*H*), 7.77 (d, J = 8.2 Hz, 1*H*), 7.61 (d, J = 8.2 Hz, 1*H*), 7.53–7.42 (m, 3*H*), 3.20 (q, J = 7.0 Hz, 1*H*), 2.81–2.65 (m, 4*H*), 1.91–1.84 (m, 4*H*), 1.45 (d, J = 7.0 Hz, 3*H*); ^{13}C-NMR (100 MHz, $CDCl_3$) δ 173.1 (C), 134.0 (C), 132.5 (C), 128.9 (CH), 126.1 (CH), 126.0 (CH), 125.8 (CH), 124.5 (CH), 119.9 (CH), 118.3 (CH), 64.2 (CH), 42.0 (CH_2), 23.5 (CH_2), 23.4 (CH_3), 16.5 (CH_3); IR (KBr): ν: 3340,03 250, 2970, 2940, 2860, 2790, 1530, 1490, 770 cm^{-1}; HRMS (ESI, m/z): Calcd for $C_{17}H_{20}N_2O$ $[M + H]^+$ 269,1654 found 269.1649; HPLC pureza = 99,0%; % ((Solución A: (TFA 0.01%/acetonitrilo)) y (Solución B: TFA 0.01%), 1 mL min^{-1}, tR = 3.390 min). Yield 82%, White solid, m.p. = 165-166 °C.

4.2 X-ray diffraction measurements

Colorless crystals of the title compounds suitable for X-ray diffraction analysis were selected and measured. Diffraction data were collected at 295(2) K on a Bruker D8 Venture diffractometer equipped with a Photon-III C14 detector, using graphite monochromated MoKα (λ = 0.71073 Å) radiation. The diffraction frames were integrated using the APEX4 package[31] and were corrected for absorptions with SADABS.[32] The crystal structures of the title compounds were solved by intrinsic phasing[6] using the OLEX2 software[33] and refined with full-matrix least-squares methods based on F^2 (SHELXL).[34] All the non-hydrogen atoms were refined with anisotropic displacement parameters. The hydrogen atoms were included from calculated positions and refined riding on their respective carbon atoms with isotropic displacement parameters. All geometrical calculations were done using the software Platon.[35]

4.3 Computational methods

The X-ray diffraction experimental results for **5a–5d** compounds were directly taken for initial molecular geometries. The geometry optimizations were carried out using the M062X exchange–correlation functional[36] and def2tzvp basis set,[37] all in gas phase. M062X is a hybrid meta exchange–correlation functional with double the nonlocal exchange (2X), which is parametrized for nonmetal and long noncovalent range interactions.[38] The calculations were performed using Gaussian 09 software.[39]

Optimized structural parameters were used to calculate theoretical electronic spectrum of **5a–5d** compounds through the time-dependent density functional theory (TDDFT) calculations[40,41] at the B3LYP/def2tzvp level of theory. The methanol solvent effect on the calculated electronic properties of the studied compound was investigated using the polarizable continuum model (PCM).[42,43]

The frontier molecular orbitals (FMOs),[44] the highest occupied molecular orbital (HOMO) and lowest unoccupied molecular orbital (LUMO), which account for the ability to donate and accept electrons, were calculated at DFT/M062X/def2tzvp level. Some global reactivity descriptors, such as HOMO–LUMO gap, chemical hardness (η), chemical potential (μ), electrophilicity index (μ), and chemical softness (s), which are based on the HOMO and LUMO energies were studied to measure the stability of synthesized molecules.

The electric dipole moment, linear polarizability, and the first and second hyperpolarizability tensors were evaluated using FF approach to explore the non-lineal optical (NLO) properties of the title compound with a field frequency of 0.0010 au at the DFT/DCAM-B3LYP/6-311G++ (d,p) level. DFT functional has shown results close to CCSD and MP2 methodologies,[45,46] showing efficiency and accuracy for calculation of second order hyperpolarizability. In the finite field (FF) method, when a molecule is subjected to a static field (F), the energy (E) of the molecule can be expressed as:

$$E = E^0 - \mu_i F_i - \frac{1}{2}\alpha_{ij}F_iF_jF_k - \frac{1}{2}\gamma_{ijkl}F_iF_jF_kF_l - \ldots$$

where E^0 is the energy of the molecule in the absence of an electronic field, μ is a part of the dipole moment vector, and it is given as:

$$\mu = (\mu_x{}^2 + \mu_y{}^2 + \mu_z{}^2)^{1/2}$$

On the other hand, α corresponds to the linear polarizability tensor, while β and γ are the first and second hyperpolarizability tensors, with i, j, and k as the labels for x, y, and z components, respectively. The tensors equations are given as follows:

$$\langle\alpha\rangle = \frac{1}{3}\left(\alpha_{xx} + \alpha_{yy} + \alpha_{zz}\right)$$

$$\langle\beta\rangle = [(\beta_{xxx} + \beta_{xyy} + \beta_{xzz})^2 + (\beta_{yyy} + \beta_{yzz} + \beta_{yxx})^2 + (\beta_{zzz} + \beta_{zxy} + \beta_{zyy})^2]^{1/2}$$

$$\langle\gamma\rangle = \frac{1}{5}\left[\gamma_{xxxx} + \gamma_{yyyy} + \gamma_{zzzz} + 2\left[\gamma_{xxyy} + \gamma_{yyzz} + \gamma_{xxzz}\right]\right]$$

Molecular docking calculations were performed to evaluate the potential affinity of the compounds on four different molecular targets; MAO-A, MAO-B, AChE and BChE. Crystallographic structures were obtained from the protein databank[47] (Table 6) and prepared using the protein preparation wizard module of the Schrödinger suite.[48,49] Hydrogen and missing atoms were added, and amino acid protonation states were assigned at pH 7.0 with PROPKA[50] software. The FAD molecule was retained for MAO-A and MAO-B and crystallized water

molecules within 5 Å of the FAD cofactor and/or co-crystallized ligands were retained for all systems. Energetic minimization was performed considering the hydrogen atoms only. Prior to molecular docking calculations, the reference ligand was removed from the binding site, but FAD molecules were retained for MAO-A and MAO-B.

The Induced Fit Docking (IFD) protocol[51,52] available in the Schrödinger suite was used for molecular docking calculations. The grid center for docking calculations was generated by selecting residues that were within 5 Å of the reference ligand in each system.

Subsequent to the IFD calculations, a re-scoring of the poses was performed with the MMGBSA method to obtain the binding free energy of the complexes. Finally, the pose with the most favorable binding free energy was chosen for all the systems. The protocol was validated by re-docking the co-crystallized reference ligands.

Author contributions

LC-A: investigation, methodology, writing – original draft; MB: computational analyses, methodology, writing – original draft; LP-P: conceptualization, methodology, writing – review & editing; EP-C: conceptualization, writing – original draft IB: Writing – original draft, visualization, software; GE. D: writing – original draft, visualization, software; WG: project administration, resources, supervision, writing – review & editing and MG: project administration, resources, supervision, writing – review & editing.

Conflicts of interest

The authors declare that the research was conducted in the absence of any commercial or financial relationships that could be construed as a potential conflict of interest.

Acknowledgements

The authors acknowledge the Research Group of the Laboratory of Organic Synthesis and Biological Activity of the University of Talca. ANID National Doctorate Scholarship 2019 Folio No. 21190020. Fondecyt Projects 1200531, 1191133 and 3210529. The authors also acknowledge to FONDEQUIP program (EQM 130021, 160063 and 180024). Gobierno Regional del Maule. FIC-R grant 40.027.577–0. This work was supported by the Universidad de Ibagué Research Fund, Ibague, Colombia, project No. 20-002-INT. FONDECYT-ANID postdoctoral grant No 3210774.

References

1 P. C. Poortvliet, K. O'Maley, P. A. Silburn and G. D. Mellick, *Front. Neurol.*, 2020, **11**, 686.
2 D. L. M. Radder, I. H. Sturkenboom, M. van Nimwegen, S. H. Keus, B. R. Bloem and N. M. de Vries, *Int. J. Neurosci.*, 2017, **127**, 930–943.
3 J. P. M. Finberg and J. M. Rabey, *Front. Pharmacol*, 2016, **7**, 340.
4 R. T. Bartus, R. L. Dean, B. Beer and A. S. Lippa, *Science*, 1982, **217**, 408–417.
5 W. Poewe, K. Seppi, C. M. Tanner, G. M. Halliday, P. Brundin, J. Volkmann, A. E. Schrag and A. E. Lang, *Nat. Rev. Dis. Primers*, 2017, **3**, 1–21.
6 V. A. Panova, S. I. Filimonov, Z. V. Chirkova, M. V. Kabanova, A. A. Shetnev, M. K. Korsakov, A. Petzer, J. P. Petzer and K. Y. Suponitsky, *Bioorg. Chem.*, 2021, **108**, 104563.
7 H. Wasan, D. Singh and R. KH, *Brain Res. Bull.*, 2021, **168**, 165–177.
8 F. Stocchi, A. Antonini, D. Berg, B. Bergmans, W. Jost, R. Katzenschlager, J. Kulisevsky, P. Odin, F. Valldeoriola and K. Ray Chaudhuri, *NPJ Parkinson's dis.*, 2022, **8**, 1–9.
9 D. Mishra, A. Fatima, P. Kumar, N. S. Munjal, B. K. Singh and R. Singh, *ChemistrySelect*, 2022, **7**, 202203060.
10 S. Hosseini, S. A. Pourmousavi, M. Mahdavi and P. Taslimi, *J. Mol. Struct.*, 2022, **1255**, 132229.
11 L. Camargo-Ayala, L. Prent-Peñaloza, E. Polo-Cuadrado, I. Brito, J. Cisterna, E. Osorio, W. González and M. Gutiérrez, *J. Mol. Struct.*, 2021, 131544.
12 W.-H. Liu, L. Guan, D.-H. Zhao, Z.-W. He, Y.-M. Hu, Y.-X. Zhu, L.-J. Zhang, L.-H. Jin, L.-P. Guan and S.-H. Wang, *SSRN Electron. J.*, 2022, 4149179.
13 V. R. Pattabiraman and J. W. Bode, *Nature*, 2011, **480**, 471–479.
14 P. W. Seavill and J. D. Wilden, *Green Chem.*, 2020, **22**, 7737–7759.
15 A. Williams and I. T. Ibrahim, *Carbodiimide Chemistry: Recent Advances*, 1981, **81**, 589–636.
16 J. R. Dunetz, J. Magano and G. A. Weisenburger, *Org. Process Res. Dev.*, 2016, **20**, 140–177.
17 A. El-Faham and F. Albericio, *Chem. Rev.*, 2011, **111**, 6557–6602.
18 A. Jordan, K. D. Whymark, J. Sydenham and H. F. Sneddon, *Green Chem.*, 2021, **23**, 6405–6413.
19 L. A. Carpino and A. El-Faham, *Tetrahedron*, 1999, **55**, 6813–6830.
20 F. H. Allen, O. Kennard, D. G. Watson, L. Brammer, A. G. Orpen and R. Taylor, *J. Chem. Soc., Perkin trans. 2*, 1987, S1–S19.
21 C. R. Groom and F. H. Allen, *Angew. Chem., Int. Ed.*, 2014, **53**, 662–671.
22 J. Bernstein, R. E. Davis, L. Shimoni and N.-L. Chang, *Angew. Chem., Int. Ed. Engl.*, 1995, **34**, 1555–1573.
23 B. Narayana, H. S. Yathirajan, R. Rathore and C. Glidewell, *Acta Crystallogr., Sect. E: Crystallogr. Commun.*, 2016, **72**, 1270–1275.
24 S.-Y. Son, J. Ma, Y. Kondou, M. Yoshimura, E. Yamashita and T. Tsukihara, *Proc. Natl. Acad. Sci. U. S. A.*, 2008, **105**, 5739–5744.
25 T. Rahman and M. Rahmatullah, *Bioorg. Med. Chem. Lett.*, 2010, **20**, 537–540.
26 C. Binda, M. Aldeco, A. Mattevi and D. E. Edmondson, *J. Med. Chem.*, 2011, **54**, 909–912.

27 F. Nachon, E. Carletti, C. Ronco, M. Trovaslet, Y. Nicolet, L. Jean and P. Y. Renard, *Biochem. J.*, 2013, **453**, 393–399.
28 C. Ronco, R. Foucault, E. Gillon, P. Bohn, F. Nachon, L. Jean and P.-Y. Renard, *ChemMedChem*, 2011, **6**, 876–888.
29 M. Ahmed, J. B. T. Rocha, M. Corrêa, C. M. Mazzanti, R. F. Zanin, A. L. B. Morsch, V. M. Morsch and M. R. C. Schetinger, *Chem.-Biol. Interact.*, 2006, **162**, 165–171.
30 I. Lukac, P. G. Wyatt, I. H. Gilbert and F. Zuccotto, *J. Comput. Aided Mol. Des.*, 2021, **35**, 1025–1036.
31 Bruker AXS INC., *APEX3, SAINT and SADABS*, Bruker AXS Inc., Madison, Wisconsin, USA, 2016.
32 G. M. Sheldrick, *SADABS, Software for Empirical Absorption Corrections*, Univ. Göttingen, Göttingen, Germany, 2000.
33 O. V Dolomanov, L. J. Bourhis, R. J. Gildea, J. A. K. Howard and H. Puschmann, *J. Appl. Crystallogr.*, 2009, **42**, 339–341.
34 G. M. Sheldrick, *Acta Crystallogr. C Struct. Chem.*, 2015, **71**, 3–8.
35 A. L. Spek, *J. Appl. Crystallogr.*, 2003, **36**, 7–13.
36 R. Krishnan, J. S. Binkley, R. Seeger and J. A. Pople, *J. Chem. Phys.*, 1980, **72**, 650–654.
37 A. Hellweg and D. Rappoport, *Phys. Chem. Chem. Phys.*, 2015, **17**, 1010–1017.
38 Y. Zhao and D. G. Truhlar, *Theor. Chem. Acc.*, 2008, **120**, 215–241.
39 G. T. Frisch, H. Schlegel, G. Scuseria, M. Robb, J. Cheeseman, J. Montgomery, T. Vreven,K. Kudin, J. Burant, J. Millam, S. Iyengar, J. Tomasi, V. Barone, B. Mennucci, M. Cossi, G. Scalmani, N. Rega, G. Petersson, H. Nakatsuji, M. Hada, M. Ehara, K. Toyota, R. Fukuda, J. Hasegawa, M. Ishida, T. Nakajima, Y. Honda, O. Kitao, H. Nakai, M. Klene, X. Li, J. Knox, H. Hratchian, J. Cross, V. Bakken, C. Adamo, J. Jaramillo, R. Gomperts, R. Stratmann, O. Yazyev, A. Austin, R. Cammi, C. Pomelli, J. Ochterski, P. Ayala, K. Morokuma, G. Voth, P. Salvador, J. Dannenberg, V. Zakrzewski, S. Dapprich, A. Daniels, M. Strain, O. Farkas, D. Malick, A. Rabuck, K. Raghavachari, J. Foresman, J. Ortiz, Q. Cui, A. Baboul, S. Clifford, J. Cioslowski, B. Stefanov, G. Liu, A. Liashenko, P. Piskorz, I. Komaromi, R. Martin, D. Fox, T. Keith, A. Laham, C. Peng, A. Nanayakkara, M. Challacombe, P. Gill, B. Johnson, W. Chen, M. Wong, C. Gonzalez and J. Pople, *Fox, Gaussian 09, Revision A.08*, Gaussian, Inc., Wallingford, 2009.
40 R. Bauernschmitt and R. Ahlrichs, *Chem. Phys. Lett.*, 1996, **256**, 454–464.
41 M. E. Casida, C. Jamorski, K. C. Casida and D. R. Salahub, *J. Chem. Phys.*, 1998, **108**, 4439–4449.
42 S. Miertuš, E. Scrocco and J. Tomasi, *Chem. Phys.*, 1981, **55**, 117–129.
43 J. L. Pascual-ahuir, E. Silla and I. Tuñon, *J. Comput. Chem.*, 1994, **15**, 1127–1138.
44 H. Chermette, *J. Comput. Chem.*, 1999, **20**, 129–154.
45 Y.-Y. Hu, S.-L. Sun, S. Muhammad, H.-L. Xu and Z.-M. Su, *J. Phys. Chem. C*, 2010, **114**, 19792–19798.
46 H.-B. Zhao, Y.-Q. Qiu, C.-G. Liu, S.-L. Sun, Y. Liu and R.-S. Wang, *J. Organomet. Chem.*, 2010, **695**, 2251–2257.
47 H. M. Berman, *Nucleic Acids Res.*, 2000, **28**, 235–242.
48 G. Madhavi Sastry, M. Adzhigirey, T. Day, R. Annabhimoju and W. Sherman, *J. Comput. Aided Mol. Des.*, 2013, **27**, 221–234.
49 N. P. P. W. E. Schrödinger, *LLC, New York, NY, Impact, Schrödinger, LLC, New York, NY, Prime, Schrödinger*, LLC, New York, 2020.
50 M. H. M. Olsson, C. R. Søndergaard, M. Rostkowski and J. H. Jensen, *J. Chem. Theory Comput.*, 2011, **7**, 525–537.
51 W. Sherman, T. Day, M. P. Jacobson, R. A. Friesner and R. Farid, *J. Med. Chem.*, 2006, **49**, 534–553.
52 N. I. F. D. P. G. Schrödinger, *LLC, New York, NY, Impact, Schrödinger, LLC, New York, NY, Prime, Schrödinger*, LLC, New York, 2020.